

SHEAR STRENGTH PREDICTION OF FRP-FRC-BEAMS WITHOUT STIRRUPS

Thiago A. Gomes, Pontifical Catholic University of Rio de Janeiro, Brazil, thiago.andg@gmail.com
Daniel C. T. Cardoso, Pontifical Catholic University of Rio de Janeiro, Brazil, dctcardoso@puc-rio.br

ABSTRACT

The current work examines the state of the art regarding design models to predict the shear strength of reinforced concrete beams with FRP bars and fiber reinforced concrete (FRC). A data base of previous experimental data was collected and the predictive capabilities of shear design models were investigated. A mechanical model based on the modified compression field theory (MCFT) was adapted for use to prediction of FRP-FRC beams shear strength. The design models performed satisfactorily, but there is a lack of experimental data with FRP-FRC beams. The MCFT-adapted model performs well and could be a viable solution that consider equilibrium, compatibility and constitutive relationships.

KEYWORDS

Fiber reinforced concrete (FRC), FRP bars, Shear design models, MCFT.

INTRODUCTION

The use of Fiber Reinforced Polymer (FRP) bars as an alternative to steel reinforcement in reinforced concrete structures has increased due to their beneficial characteristics. FRP is a non-corrosive, electrically non-conductive, and non-magnetic composite material. While FRP bars have higher tensile strength, they may exhibit lower elastic modulus (depending on the impregnated fiber), deformation capacity, and linear-elastic behavior which increases the sensitivity of FRP-RC beams to the service limit state (Nanni et al., 2014). To enhance the performance of reinforced concrete (RC) beams with FRP bars, Fiber-Reinforced Concrete (FRC) has been investigated. In terms of shear behavior, FRC has shown to enhance shear strength, ductility, and energy absorption in FRP-FRC beams (Dev et al., 2020; Gomes et al., 2023; Hosseini et al., 2021; Muhammad & Yousif, 2023; Tran et al., 2020; Vakili et al., 2019). However, the development of reliable models for estimating shear strength of FRP-FRC-beams is required.

Shear failure of RC beams typically happens in a plastic condition, i.e. after cracking. Aggregate interlock (V_{ag}), dowel effect (V_d), concrete residual strength throughout the fracture processing zone (V_{res}) and force transfer through compression chord (V_{cc}) act together as shear-transfer mechanisms during loading (Cavagnis, 2017). In code design models, these mechanisms are typically accounted as the shear resistance component provided by concrete (V_c). Additionally, FRP stirrups and fibers can be used as shear reinforcement. Gomes et al. (2023) examined the shear behavior of GFRP-FRC beams. The primary goal of this study was to analyze the action of shear-transfer mechanisms in GFRP-FRC beams with and without GFRP stirrups and basalt fibers. Digital image correlation (DIC) was used to monitor the displacement fields throughout the shear span, and literature-based shear-transfer constitutive models were used to calculate the relative importance of each contributing mechanism. According to the findings, FRP stirrups and fibers existence must be considered when quantifying the contributions of the other mechanisms because they mechanically interact while the beam is loaded and, depending on the level of deformation, they may have limited contributions to the shear strength.

Shear behavior of fiber reinforced concrete beams without stirrups was recently analyzed critically by Lantsoght (2019). According to the research, “a number of existing equations are based on the combination of a concrete contribution and a contribution of the steel fibers to the shear capacity. When

the concrete contribution is based on an empirically determined inclined cracking load and the contribution of the steel fibers on the capacity of fibers under tension crossing the crack, the resulting equations mix concepts that mechanically do not work together”. Unlike empirical models, the modified compression field theory (MCFT) uses the strain conditions in the web to determine the inclination θ of the diagonal compressive stresses taking into account equilibrium, compatibility, and constitutive relationships in terms of average stresses and strains (Bentz et al., 2006).

Some research has presented empirical shear models to analyze the shear strength of FRP-FRC beams (Hosseini et al., 2021), while others have adapted code models of steel-FRC beams (Dev et al., 2020; Tran et al., 2020). In addition, a model based on the MCFT approach was also presented as a possible solution (Tran et al., 2020). Nonetheless, the methods have been used to predicting the shear strength of the experimental data generated by the same studies. Therefore, the goal of this study is to examine the models for predicting shear in FRP-FRC beams that have been proposed in recent research and to analyze a potential solution of a shear design model based on the MCFT with modification based in previous studies.

DATABASE

A database of experimental test in FRP-FRC beams that failed by shear was collected from the following studies: Dev et al. (2020); Gomes et al. (2023); Hosseini et al. (2021); Muhammad & Yousif (2023); Tran et al. (2020); Vakili et al. (2019). Only samples providing sufficient data for the design model predictions discussed in the following section were taken into account. The complete database is presented in Appendix A. Figure 1 presents the effective depth (d), concrete compressive strength (f'_c), flexural reinforcement index ($E_f \rho_f$) and concrete type covered by the database.

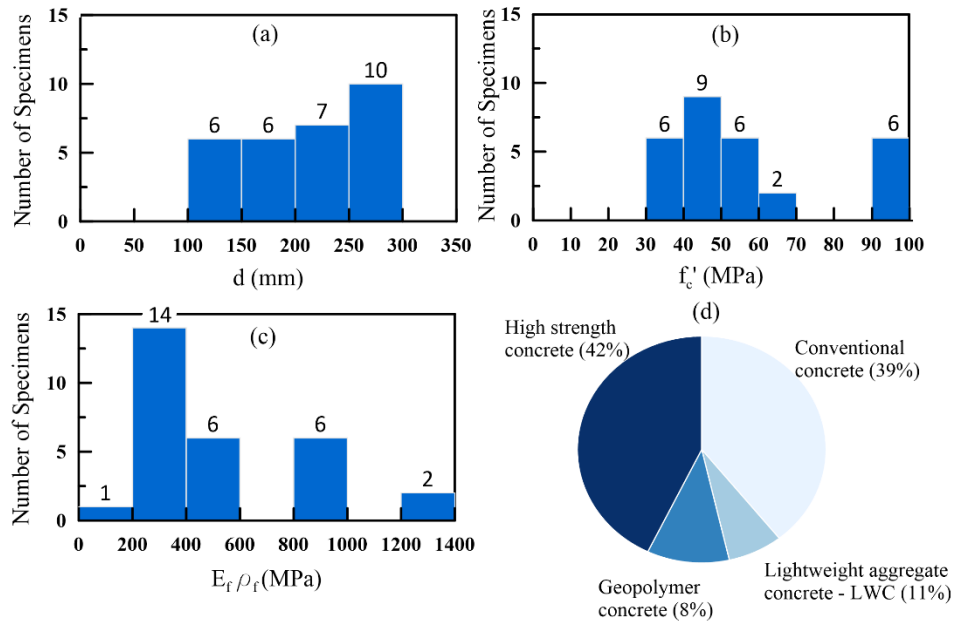


Figure 1: Number of specimens according to: effective depth (a), concrete compressive strength (b), flexural reinforcement index (c) and concrete type (d).

SHEAR STRENGTH DESIGN MODELS

Figure 2 shows the shear modeling variables usually considered in design models for FRC beams. In general, the shear strength is given by the sum of the resistance of concrete (V_c) and the shear resistance of fibers (V_{fib}). Table 1 shows models that have been used in literature studies towards predicting the shear strength of FRP-FRC beams. Detailed descriptions of the variables can be found in this paper's symbol list. The presented models can be summarized as follows:

Table 1: Summary of FRC-FRP beams shear-design models used in previous studies.

<p>Model 1 (Dev et al., 2020)</p>	$V_{c1} = \frac{2}{5}\sqrt{f'_c}bc \text{ where } c = kd \text{ and } k = \sqrt{2\rho_f n_f + (\rho_f n_f)^2} - \rho_f n_f \quad (\text{Eq. 1})$ $V_{fib1} = 0.7k_1\tau_{fd}bd \quad (\text{Eq. 2})$ $k_1 = 1 + \sqrt{\frac{200}{d}} \leq 2 \quad (\text{Eq. 3})$ $\tau_{fd} = 0.12f_{R,4} \quad (\text{Eq. 4})$ $V_{u1} = V_c + V_{fib} \quad (\text{Eq. 5})$
<p>Model 2 (Dev et al., 2020)</p>	$V_{u2} = \frac{0.18}{\gamma_c} k_s \left[100\rho \left(1 + 7.5 \frac{\sigma_{f2}}{f_{ctk}} \right) f_{ck} \right]^{1/3} bd \text{ where } k_s = 1 + \sqrt{\frac{200}{d}} \leq 2 \quad (\text{Eq. 6})$ $\sigma_{f2} = 0.45f_{R,1} - \frac{1.5}{2.5} (0.45f_{R,1} - 0.5f_{R,3} + 0.2f_{R,1}) \geq 0 \quad (\text{Eq. 7})$
<p>Model 3 (Tran et al., 2020)</p>	$V_{c3} = \frac{2}{5}\sqrt{f'_c}bc \text{ where } c = kd \text{ and } k = \sqrt{2\rho_f n_f + (\rho_f n_f)^2} - \rho_f n_f \quad (\text{Eq. 8})$ $E_c = 4700\sqrt{f'_c} \text{ for conventional concrete} \quad (\text{Eq. 9})$ $E_c = 3510\sqrt{f'_c} \text{ for Geopolymer concrete}$ $V_{fib3} = 0.9db\sigma_f \quad (\text{Eq. 10})$ <p>for steel fibers:</p> $\sigma_{f3} = 0.41\beta\tau_b V_f \frac{l_f}{d_f} \begin{cases} \tau_b = 0.68\sqrt{f'_c} \text{ for conventional concrete (OPC)} \\ \tau_b = 1.21\sqrt{f'_c} \text{ for geopolymer concrete (GPC)} \end{cases} \quad (\text{Eq. 11})$ <p>Others types of fibers (Mobasher et al., 2014):</p> $\sigma_{f3} = 0.3f_{R,3} \text{ when available results from Model Code (2013) bending test.} \quad (\text{Eq. 12})$ $\sigma_{f3} = 0.33f_{150}^D \text{ when available results from C1609/C1609M-19a (2019) bending test.}$ $V_{u3} = V_c + V_{fib} \quad (\text{Eq. 13})$
<p>Model 4 (Tran et al., 2020)</p>	$V_{c4} = \left(\frac{\rho_f E_f}{90\beta_1 f'_c} \right)^{1/3} \left(\frac{\sqrt{f'_c} bd}{6} \right) \begin{cases} \beta_1 = 0.85 - 0.05 \frac{f'_c - 28}{7} \geq 0.65 \text{ (OPC)} \\ \beta_1 = -0.00254f'_c + 0.8675 \geq 0.7 \text{ (GPC)} \end{cases} \quad (\text{Eq. 14})$ $V_{u4} = V_c + V_{fib3} \text{ where } V_{fib3} \text{ is computed similarly as model 3} \quad (\text{Eq. 15})$

- Model 1: The shear strength (V_{u1}) is given by the sum of the shear resistance of concrete (V_{c1}) defined by ACI 440.1R-15 and the shear resistance of fibers (V_{fib1}) defined by the recommendation of RILEM TC-162 (Vandewalle, 2003).
- Model 2: The shear strength (V_{u2}) is calculated using a single shear equation of ACI 544.4R-18 (2018) with a modification in the reinforcement ratio (ρ) that is replaced by an equivalent steel reinforcement ratio to account for the use FRP bars as the longitudinal reinforcement. The residual strength of the fibers is calculated with the linear-model fib Model Code 2010 (Model Code, 2013).
- Model 3: The shear strength (V_{u3}) is given by the sum of the shear resistance of concrete (V_{c3}) defined by ACI 440.1R-15 and the shear resistance of fibers (V_{fib3}) given by the vertical projection of the fibers contribution through the crack considering the inclination θ of the diagonal compressive stresses equal to 45° .
- Model 4: The shear strength (V_{u4}) is given by the sum of the shear resistance of concrete (V_{c4}) defined by Ahmed K. El-Sayed et al., 2006 and the shear resistance of fibers (V_{fib4}) given by the vertical projection of the fibers contribution through the crack considering the inclination θ of the diagonal compressive stresses equal to 45° .

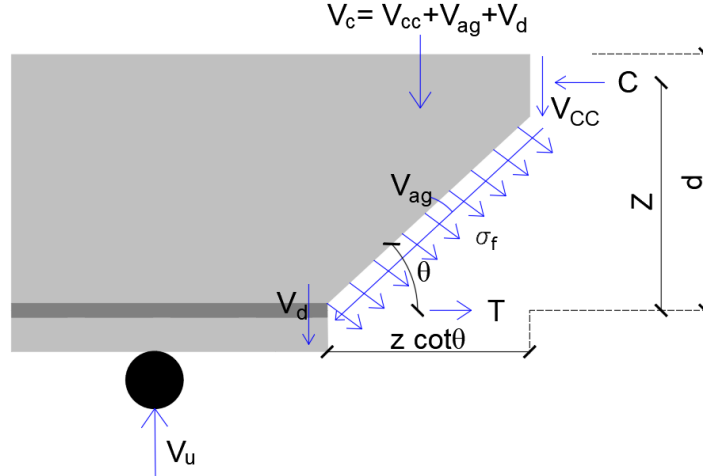


Figure 2: Shear modeling variables (Adapted from Khuntia et al., 1999).

Model 5: MCFT approach

Based on previous studies that used MCFT to proposed shear-strength equations for FRC-beams (Amin & Foster, 2016; Stephen Foster, 2010; Tran et al., 2020), this paper presents a MCFT design model that considers the impact of fibers in FRP-FRC-beams without stirrups with the appropriate application of the constitutive behavior of FRC obtained in the three point bending test. According to the MCFT adapted to FRP-RC beams (Bentz et al., 2010; Hoult et al., 2008), the shear resistance provided by concrete (Figure 2) is calculated as follows:

$$V_{cs} = \frac{0.30}{0.5 + (1000\varepsilon_x + 0.15)^{0.7}} \times \frac{1300}{(1000 + s_{xe})} \sqrt{f'_c} \times bd \quad (\text{Eq. 16})$$

where, ε_x is the mid-depth longitudinal strain and s_{xe} is the effective crack spacing that is a function of the maximum specified coarse aggregate size (a_g) and the size of the member (Bentz et al., 2010).

$$s_{xe} = \frac{31.5d}{16 + a_g} \geq 0.77d \quad (\text{Eq. 17})$$

For lightweight and high-strength concrete (HSC), cracks tend to pass through the aggregate rather than around them, resulting in smoother crack surfaces with reduced aggregate interlock capacity. In such cases, a_g is assumed as zero. In this study, high-strength concrete is defined as having a compressive strength greater than 50 MPa. The mid-depth longitudinal strain is conservatively approximated by half the strain in the flexural tensile reinforcement for members without axial load or prestressing, as determined by a simple truss model (Amin & Foster, 2016; Stephen Foster, 2010; Tran et al., 2020):

$$\varepsilon_x = \frac{M/z + 0.5V_{u5} \cot \theta}{2E_f A_f} \quad (\text{Eq. 18})$$

where z is the internal moment lever arm, and M and V_{u5} correspond to moment and shear in the critical section, respectively. As adopted by Trun et al. (2020), in this study the moment in the critical section was considered equal to $(a - z \cot \theta)V_{u5}$, where a is the shear span length. Unlike previous studies by Foster (2010) and Amin and Foster (2016), which used a linear approximation, the crack width at the mid-height of the section, w , should be taken as a "second-order" approximation due to a larger margin for larger strains in FRP-beams (Hoult et al., 2008).

$$w = 0.9 \cdot (0.15 + 1000\varepsilon_x)^{0.7} \quad (\text{Eq. 19})$$

The MCFT predicts the angle of the principal compressive stress, or strut angle θ , at shear failure for members with shear reinforcement to depend primarily upon the longitudinal strain ε_x .

$$\theta = (29^\circ + 7,000\varepsilon_x) \left(0.88 + \frac{s_{xe}}{2,500} \right) \leq 75^\circ \quad (\text{Eq. 20})$$

The critical crack width and longitudinal strain affect the fibers' shear strength (Figure 2). Fiber contribution averaged over the failure surface is given by:

$$V_{fib5} = k_{fd} \sigma_{f5} b z \cot \theta \quad (\text{Eq. 21})$$

where k_{fd} is the fiber dispersion reduction factor, taken as $k_{fd} = 0.82$. This factor takes into account the possible crack path deviations near fiber ends in cases where the crack location cannot be predicted (Foster, 2010). The residual tensile strength is given by the linear post-cracking constitutive model defined by fib Model Code (2010).

$$\sigma_{f5} = 0.45f_{R,1} - \frac{w}{2.5} (0.45f_{R,1} - 0.5f_{R,3} + 0.2f_{R,1}) \geq 0 \quad (\text{Eq. 22})$$

Overall, the total shear resisted by the concrete mechanisms and fibers is given by:

$$V_{u5} = V_{c5} + V_{fib5} \quad (\text{Eq. 23})$$

Since both the fiber and concrete contribution at the critical section must be calculated as function of ε_x , an iterative procedure must be used to solve the shear capacity of the FRP-FRC beams. The iterative solution is a comoom approach to design models based on MCFT (Bentz et al., 2010; Bentz & Collins, 2006; Hoult et al., 2008). Assuming an initial ε_x , eq. 16-23 should be used to calculate V_{u5} . Then, using this result, a new value of ε_x is calculated; if it differs from the initial value, a new value of V_{u5} must be calculated. The procedure must be repeated until convergence is reached. It can be created through programming or by using a simple spreadsheet. Typically, a fast convergence is obtained. To analyze

the beams without results from three point bending test method of fib Model Code (2013), the residual tensile strength was considered as the alternative equations presented in table 1 (Model 3). In this case, model 5 was used without considering σ_f variation with the compatibility deformation equations (Eq. 19).

RESULTS

In some cases, the lack of necessary design model properties for a beam prevented the utilization of this particular model in predicting the shear strength. Thus, 13 beams were examined using models 1 and 2, and 29 beams were examined using models 3, 4, and 5. Thus, 13 beams were examined using models 1 and 2, and 29 beams were examined using models 3, 4, and 5.

Table 2 and Figure 4 show the relation between the experimental shear-strength of the data base specimens and the prediction shear-strength by models 1-5 (V_{u1} , V_{u2} , V_{u3} , V_{u4} , V_{u5}). After analyzing the predictive capabilities of models 1 and 2, it is evident that they resulted in a more conservative approach compared to the other applied models, with average values of V_{exp}/V_{u1} and V_{exp}/V_{u2} of 1.89 and 1.98, respectively. Model 3 showed a better performance than models 1 and 2, exhibiting an average value of 1.41 and a standard deviation of 0.28. The most noteworthy performances were observed with the implementation of models 4 and 5, which yielded average values of 1.20 and 1.34, respectively, accompanied by standard deviations of 0.22 and 0.25. However, it is worth mentioning that approximately 21% of the beams analyzed using model 4 yielded unconservative results.

Figure 4 shows an analysis of strength prediction for model 5 (V_{exp}/V_{u5}) that highlights the beams that did not have the results of a three-point bending test. In this analysis, a simplification of model 5 was used as previously described, i.e. the variation of σ_f with the compatibility deformation equations was not taken into account. Furthermore, it is expected that the results of a three point bending test will provide better results than empirical equations used for beams with steel fibers. Figure 3 exclusively displays the outcomes of applying model 5 to beams with three-point bending test results. It is evident that the model exhibited superior performance in predicting the shear strength for these beams. Consequently, it holds promising potential as a viable solution for the design of FRP-FRC beams, requiring further investigations.

The proposed models, in most of the cases, led to conservative results in the prediction of the shear strength in the database. However, there is still a lack of knowledge on the quality of the predictions to different situations that are not included in the limited experimental tests available. In general, the reliability of the models should be analyzed not only to describe this limited experimental data but also to account for the parameters that governs the kinematic crack behavior and the shear-transfer actions in beams.

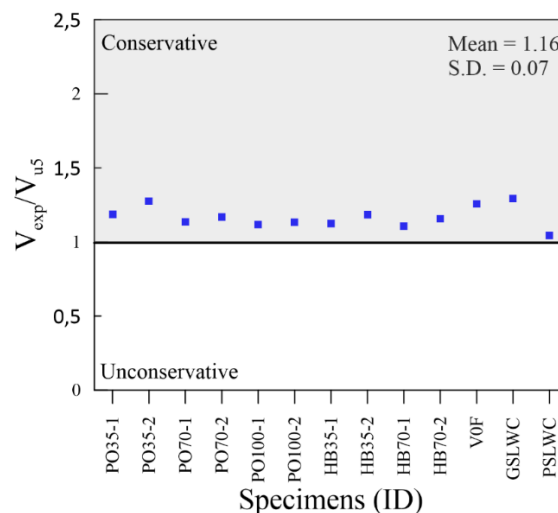


Figure 3: Prediction of shear strength by model 5 of specimens with three point bending test results.

Table 2: Ratio between the experimental shear strength and predicted shear strength by models 1-5.

Researcher	Specimens (ID)	Vexp/Vu1	Vexp/Vu2	Vexp/Vu3	Vexp/Vu4	Vexp/Vu5
Dev et al., 2020	PO35-1	2.21	2.04	1.68	1.32	1.19
	PO35-2	2.37	2.19	1.80	1.42	1.28
	PO70-1	1.74	2.07	1.19	1.02	1.14
	PO70-2	1.79	2.13	1.23	1.05	1.17
	PO100-1	1.61	2.02	1.01	0.89	1.12
	PO100-2	1.63	2.05	1.02	0.90	1.13
	HB35-1	2.05	1.94	1.49	1.20	1.12
	HB35-2	2.16	2.04	1.57	1.26	1.18
	HB70-1	1.66	1.97	1.07	0.93	1.11
	HB70-2	1.73	2.06	1.11	0.97	1.16
Gomes et al., 2023	V0F	2.39	2.02	1.60	1.33	1.26
Vakili et al., 2019	GSLWC	1.71	1.75	1.44	1.14	1.29
	PSLWC	1.55	1.45	1.08	0.88	1.04
Tran et al., 2020	OPC-SF0.5	N.A.	N.A.	1.51	1.28	1.36
	GPC-SF0.25	N.A.	N.A.	1.24	1.12	1.07
	GPC-SF0.5	N.A.	N.A.	1.30	1.22	1.35
	GPC-SF1	N.A.	N.A.	0.79	0.76	1.07
Hosseini et al., 2021	S2.5-G10-SF0.75-R0	N.A.	N.A.	1.80	1.52	1.67
	S2.5-G10-SF1.5-R0	N.A.	N.A.	1.30	1.16	1.63
	S2.5-G10-SF0.75-R5	N.A.	N.A.	1.55	1.30	1.42
	S2.5-G10-SF1.5-R5	N.A.	N.A.	1.13	1.01	1.40
	S2.5-G10-SF0.75-R10	N.A.	N.A.	1.71	1.44	1.55
	S2.5-G6-SF0.75-R10	N.A.	N.A.	1.56	1.29	1.94
Muhammad & Yousif, 2023	C90-0.75-0.71	N.A.	N.A.	1.68	1.39	1.64
	C90-1.5-0.71	N.A.	N.A.	1.42	1.24	1.81
	C90-0.75-1.71	N.A.	N.A.	1.56	1.33	1.30
	C90-1.5-1.71	N.A.	N.A.	1.64	1.45	1.63
	C90-0.75-2.52	N.A.	N.A.	1.55	1.34	1.24
	C90-1.50-2.52	N.A.	N.A.	1.83	1.64	1.70

N.A.: Not applicable due to the lack of data requested by the design model.

CONCLUSIONS

In this study, a database of FRP-FRC beams that failed due to shear force was collected and the predictive capabilities of shear strength mechanical models used in previous studies were examined. A mechanical model based on MCFT approach was adapted for use in FRP-FRC beams and was also used to analyze the experimental data. The following conclusions can be drawn from this research:

- Models 1 and 2 produced the most conservative results. Model 4 performed better in terms of average and standard deviation, however, the model also produced unconservative results in 21% of the cases under consideration.
- The adapted MCFT model for prediction of shear strength of FRP-FRC beams produced a satisfactory result, with improved performance in analyzing beams with results from three-point bending characterization tests and taking into account the variation of fiber contribution according to the compatibility deformation equation.

- The models investigated, in most of the cases, led to conservative results in the prediction of the shear strength in the database. However, there is still a lack of knowledge of the quality of the predictions to different situations that are not included in the limited experimental tests available.

ACKNOWLEDGEMENT

This study was partially financed by the Coordenação de Aperfeiçoamento de Pessoal de Nível Superior – CAPES, Finance Code 001 – and Brazilian agencies FAPERJ and CNPq.

CONFLICT OF INTEREST

The authors declare that they have no conflicts of interest associated with the work presented in this paper.

DATA AVAILABILITY

All necessary data is presented in this paper.

LIST OF SYMBOLS

$\frac{l_f}{d_f}$	fiber aspect ratio (fiber length/fiber diameter)
A_f	area of FRP longitudinal reinforcement
E_c	modulus of elasticity of concrete
E_f	modulus of elasticity of FRP bars
V_{exp}	experimental shear strength
$V_{c1}, V_{c3}, V_{c4}, V_{c5},$	Concrete contribution to the shear strength by models 1, 2, 3, 4, and 5, respectively
V_f	Volume fraction of fibers
$V_{fib1}, V_{fib3}, V_{fib4}, V_{fib5}$	Fibers contribution to the shear strength by models 1, 2, 3, 4, and 5, respectively
$V_{u1}, V_{u2}, V_{u3}, V_{u4}, V_{u5}$	shear strength predictions by models 1, 2, 3, 4, and 5, respectively
a_g	maximum diameter of the aggregate used for concrete production
f_{150}^D	residual flexural tensile strength at deflection $L/150$ measured from ASTM C1609/C1609M-19 test method
$f_{R,1}, f_{R,3}$ and $f_{R,4}$	Post-cracking residual strength obtained in three-point bending tests crack opening in the notch (CMOD) equal to 0.5, 2.5 and 3.5 mm; respectively.
f'_c	concrete compressive strength
n_f	Ratio E_c/E_f
s_{xe}	effective crack spacing
ε_x	longitudinal strain at mid-depth of the section
ρ_f	longitudinal FRP reinforcement ratio
$\sigma_{f2}, \sigma_{f3}, \sigma_{f5}$	Residual tensile strength of FRC by models 2, 3 and 5
τ_b	interface bond strength between fiber and matrix
τ_{fd}	shear strength due to fibers
a	shear span
M	acting bending moment at the critical section
b	beam's width
d	effective concrete depth
w	crack width
θ	inclination of the diagonal compressive stresses

APPENDIX A: DATABASE

Researcher	Specimens (ID)	b (mm)	d (mm)	a/d	Concrete type	ag (mm)	fc' (MPa)	Bar type	Ef (GPa)	f _{tu} (Mpa)	ρf (%)	fiber type	Vf (%)	L/d	f _{R,1} (MPa)	f _{R,3} (MPa)
Dev et al., 2020	PO35-1	250	272.7	2.2	NSC	20	41.5	GFRP	53.5	848	0.66	PO	0.35	100	1.61	1.12
	PO35-2	250	272.7	2.2	NSC	20	41.5	GFRP	53.5	848	0.66	PO	0.35	100	1.61	1.12
	PO70-1	250	272.7	2.2	NSC	20	40.4	GFRP	53.5	848	0.66	PO	0.7	100	1.85	2.53
	PO70-2	250	272.7	2.2	NSC	20	40.4	GFRP	53.5	848	0.66	PO	0.7	100	1.85	2.53
	PO100-1	250	272.7	2.2	NSC	20	41.8	GFRP	53.5	848	0.66	PO	1	100	2.96	3.47
	PO100-2	250	272.7	2.2	NSC	20	41.8	GFRP	53.5	848	0.66	PO	1	100	2.96	3.47
	HB35-1	250	272.7	2.2	NSC	20	39.4	GFRP	53.5	848	0.66	PO + steel	0.35	100/50	1.83	1.32
	HB35-2	250	272.7	2.2	NSC	20	39.4	GFRP	53.5	848	0.66	PO + steel	0.35	100/50	1.83	1.32
	HB70-1	250	272.7	2.2	NSC	20	39.8	GFRP	53.5	848	0.66	PO + steel	0.7	100/50	2.76	2.94
	HB70-2	250	272.7	2.2	NSC	20	39.8	GFRP	53.5	848	0.66	PO + steel	0.7	100/50	2.76	2.94
Gomes et al., 2023	V0F	130	224	2.5	NSC	12.5	42	GFRP	50	1000	1.17	basalt	0.5	71	2.42	1.68
Vakili et al., 2019	GSLWC	100	170	3.24	LWC	0	44	GFRP	49.4	597	0.59	glass+steel	0.3/ 0.25	789.47/ 66.66	0.35	1.21
	PSLWC	100	170	3.24	LWC	0	36	GFRP	49.4	597	0.59	POP+steel	0.80/ 0.25	521.7/ 66.66	0.30	1.44
Tran et al., 2020	OPC-SF0.5	150	168	3.27	HSC	0	66	BFRP	55	1100	1.60	Steel	0.5	64	NR	NR
	GPC-SF0.25	150	168	3.27	GPC	10	34.8	BFRP	55	1100	1.60	Steel	0.25	64	NR	NR
	GPC-SF0.5	150	168	3.27	GPC	10	42	BFRP	55	1100	1.60	Steel	0.5	64	NR	NR
	GPC-SF1	150	168	3.27	GPC	10	51	BFRP	55	1100	1.60	Steel	1	64	NR	NR
Hosseini et al., 2021	S2.5-G10-SF0.75-R0	150	120	2.5	HSC	0	64	GFRP	49.8	1015	0.89	steel	0.75	50	NR	NR
	S2.5-G10-SF1.5-R0	150	120	2.5	HSC	0	59	GFRP	49.8	1015	0.89	steel	1.50	50	NR	NR
	S2.5-G10-SF0.75-R5	150	120	2.5	HSC	0	58	GFRP	49.8	1015	0.89	steel	0.75	50	NR	NR
	S2.5-G10-SF1.5-R5	150	120	2.5	HSC	0	55	GFRP	49.8	1015	0.89	steel	1.50	50	NR	NR
	S2.5-G10-SF0.75-R10	150	120	2.5	HSC	0	54	GFRP	49.8	1015	0.89	steel	0.75	50	NR	NR
	S2.5-G6-SF0.75-R10	150	120	2.5	HSC	0	54	GFRP	49.95	1026	0.34	steel	0.75	50	NR	NR
Muhammad & Yousif, 2023	C90-0.75-0.71	150	212	3.0	HSC	0	90.25	BFRP	52	1165	0.71	basalt	0.75	66	NR	NR
	C90-1.5-0.71	150	212	3.0	HSC	0	90.18	BFRP	52	1165	0.71	basalt	1.5	66	NR	NR
	C90-0.75-1.71	150	212	3.0	HSC	0	90.25	BFRP	52	1128	1.71	basalt	0.75	66	NR	NR
	C90-1.5-1.71	150	212	3.0	HSC	0	90.18	BFRP	52	1128	1.71	basalt	1.5	66	NR	NR
	C90-0.75-2.52	150	212	3.0	HSC	0	90.25	BFRP	52	1128	2.52	basalt	0.75	66	NR	NR
	C90-1.50-2.52	150	212	3.0	HSC	0	90.18	BFRP	52	1128	2.52	basalt	1.5	66	NR	NR

NSC: Normal strength concrete; LWC: lightweight concrete; HSC: high strength concrete.

PO: Macrosynthetic polyolefin; POP: polypropylene.

GFRP: glass fiber reinforced polymer bars; BFRP: Basalt fiber reinforced polymer bar.

REFERENCES

- ASTM C1609/C1609M-19a. (2019). *Standard Test Method for Flexural Performance of Fiber-Reinforced Concrete (Using Beam With Third-Point Loading) 1*.
https://doi.org/10.1520/C1609_C1609M-19A
- ACI 440.1R-15, (2015). *Guide for the Design and Construction of Structural Concrete Reinforced with FRP Bars*.
- ACI 544.4R-18. (2018). *Guide to Design with Fiber-Reinforced Concrete*.
- Ahmed K. El-Sayed, Ehab F. El-Salakawy, & Brahim Benmokrane. (2006). Shear Strength of FRP-Reinforced Concrete Beams without Transverse Reinforcement. *ACI STRUCTURAL JOURNAL*, 103-S25, 235–243.
- Amin, A., & Foster, S. J. (2016). Shear strength of steel fibre reinforced concrete beams with stirrups. *Engineering Structures*, 111, 323–332. <https://doi.org/10.1016/j.engstruct.2015.12.026>
- Bentz, E. C., & Collins, M. P. (2006). Development of the 2004 Canadian Standards Association (CSA) A23.3 shear provisions for reinforced concrete. *Canadian Journal of Civil Engineering*, 33(5), 521–534. <https://doi.org/10.1139/L06-005>
- Bentz, E. C., Massam, L., & Collins, M. P. (2010). Shear Strength of Large Concrete Members with FRP Reinforcement. *Journal of Composites for Construction*, 14(6), 637–646.
[https://doi.org/10.1061/\(asce\)cc.1943-5614.0000108](https://doi.org/10.1061/(asce)cc.1943-5614.0000108)
- Code, fib M. (2013). fib Model Code for Concrete Structures 2010. *Fib Model Code for Concrete Structures 2010*, 1–402. <https://doi.org/10.1002/9783433604090>
- Dev, A., Chellapandian, M., & Prakash, S. S. (2020). Effect of Macrosynthetic and Hybrid Fibers on Shear Behavior of Concrete Beams Reinforced with GFRP Bars. *Journal of Bridge Engineering*, 25(7), 04020031. [https://doi.org/10.1061/\(asce\)be.1943-5592.0001557](https://doi.org/10.1061/(asce)be.1943-5592.0001557)
- Gomes, T. A., Lima De Resende, T., Carlos, D., & Cardoso, T. (2023). Shear-transfer mechanisms in reinforced concrete beams with GFRP bars and basalt fibers. *Engineering Structures*, 289, 116299. <https://doi.org/10.17632/zjtxbogg4p.1>
- Hosseini, S. A., Nematzadeh, M., & Chastre, C. (2021). Prediction of shear behavior of steel fiber-reinforced rubberized concrete beams reinforced with glass fiber-reinforced polymer (GFRP) bars. *Composite Structures*, 256(September 2020), 113010.
<https://doi.org/10.1016/j.compstruct.2020.113010>
- Hoult, N. A., Sherwood, E. G., Bentz, E. C., & Collins, M. P. (2008). Does the Use of FRP Reinforcement Change the One-Way Shear Behavior of Reinforced Concrete Slabs? *Journal of Composites for Construction*, 12(2), 125–133. [https://doi.org/10.1061/\(asce\)1090-0268\(2008\)12:2\(125\)](https://doi.org/10.1061/(asce)1090-0268(2008)12:2(125))
- Vandewalle. (2003). RILEM TC 162-TDF: ‘Test and design methods for steel fibre reinforced concrete.’ *Materials and Structures / Matériaux et Constructions*, 36, 560–567.
- Madhusudan Khuntia, Bozidar Stojadinovic, & Subhash C. Goel. (1999). Shear Strength of Normal and High-Strength Fiber Reinforced Concrete Beams without Stirrups. *ACI Structural Journal*, 96-S31, 282–289.
- Mobasher, B., Bakhshi, M., & Barsby, C. (2014). Backcalculation of residual tensile strength of regular and high performance fiber reinforced concrete from flexural tests. *Construction and Building Materials*, 70, 243–253. <https://doi.org/10.1016/j.conbuildmat.2014.07.037>
- Model Code 2010. (2013). *fib Model Code for Concrete Structures 2010*. International Federation for Structural Concrete (fib).
- Muhammad, J. H., & Yousif, A. R. (2023). Effect of basalt minibars on the shear strength of BFRP-reinforced high-strength concrete beams. *Case Studies in Construction Materials*, 18. <https://doi.org/10.1016/j.cscm.2023.e02020>
- Nanni, A., De Luca, A., & Jawaheri Zadeh, H. (2014). Reinforced Concrete with FRP Bars. In *Reinforced Concrete with FRP Bars*. <https://doi.org/10.1201/b16669>
- Stephen Foster. (2010). Design of FRC beams for shear using the VEM and the draft model code approach. In *fib bull*. International Federation for Structural Concrete.
- Tran, T. T., Pham, T. M., & Hao, H. (2020). Effect of hybrid fibers on shear behaviour of geopolymer concrete beams reinforced by basalt fiber reinforced polymer (BFRP) bars without stirrups. *Composite Structures*, 243, 112236. <https://doi.org/10.1016/j.compstruct.2020.112236>

Vakili, S. E., Homami, P., & Esfahani, M. R. (2019). Effect of fibers and hybrid fibers on the shear strength of lightweight concrete beams reinforced with GFRP bars. *Structures*, 20(January), 290–297. <https://doi.org/10.1016/j.istruc.2019.04.006>